Limnol. Oceanogr., 42(5, part 2), 1997, 1178–1188

Toxin variability during the cell cycle of the dinoflagellate *Alexandrium fundyense*

Gaspar Taroncher-Oldenburg,[1] *David M. Kulis, and Donald M. Anderson*
Biology Department, Woods Hole Oceanographic Institution, Woods Hole, Massachusetts 02543

Abstract

Cultures of the toxic dinoflagellate *Alexandrium fundyense* Balech were subjected to conditions that induced two synchronized divisions over a period of 48 h. Before, during, and after this interval, toxin content, toxin composition, and several other physiological parameters were monitored every 2 h for 94 h. Toxin production was discontinuous, induced by light, and always occurred during a defined time frame within the G_1 phase of the cell cycle. Specific toxin production rates were positive for a period of ~8–10 h in early G_1 and dropped to zero for the remainder of the interphase and mitosis. Analysis of toxin composition showed that cellular concentrations of all the saxitoxin derivatives followed a similar pattern of increase, stabilization, and decrease throughout one generation time. A putative sequence of interconversions between the derivatives could be established, with C2 as the first compound to appear. Division of a subset of the population during the first 24 h of the experiment and the ensuing total synchrony of the culture suggest the existence of two transition points in the cell cycle of this dinoflagellate. The first transition point, at the beginning of G_1, is light-dependent and holds the cells in a G_0-like period. The second block point at the end of G_1 is size-dependent and arrests the cells in G_1. We propose a model of the cell cycle of *A. fundyense* in which progression through the cell cycle can be arrested at two different transition points located in G_1 and toxin production is induced by light during G_1. The restriction of toxin production to a relatively short segment of the cell cycle provides a tool for comparing cells that are and are not synthesizing toxin.

Dinoflagellate species in the genus *Alexandrium* are responsible for paralytic shellfish poisoning (PSP) along the northeastern coast of the U.S. and Canada (Maranda et al. 1985; Cembella et al. 1987; Anderson 1989), as well as other temperate littoral waters throughout the world (Hallegraeff 1993). PSP is caused by saxitoxin (STX), a potent neurotoxin produced by some *Alexandrium* species, and >20 known STX derivatives that differ in structure and toxicity (Shimizu 1993). An important characteristic of the STX-producing dinoflagellates is that the toxicity of a single isolate can vary dramatically under different growth conditions. This variability is largely due to changes in toxin content (the integrated potency or total molar content of toxin per cell) during various stages of growth (Hall 1982; Boyer et al. 1987; Anderson et al. 1990*b*), but it can also reflect changes in toxin composition (the relative concentrations of the different STX derivatives) (Boczar et al. 1988; Anderson et al. 1990*a*).

Most studies to date have examined the toxin content of dinoflagellates on time scales of days to weeks using batch cultures. These studies have shown that toxin content varies with nutrient limitation (Hall 1982; Boyer et al. 1987; Anderson 1990) and with changes in salinity (White 1978), temperature (Hall 1982; Ogata et al. 1987; Anderson et al. 1990*b*), or light intensity (Ogata et al. 1987). A typical pattern, observed for all these conditions except phosphorous limitation, is that toxin content is highest in early exponential growth and decreases as the cells enter stationary phase (Boyer et al. 1987; Boczar et al. 1988; Anderson et al. 1990*b*). Furthermore, the specific toxin production rates were directly proportional to specific growth rates, suggesting that toxin synthesis might be linked to cell cycle events (Anderson et al. 1990*b*).

Dinoflagellates have several characteristics, such as permanently condensed chromosomes and the absence of histones that place them as a unique group among the eucaryotes (Rizzo 1987, 1991). However, recent evidence also suggests that their cell cycle is controlled by universal eucaryotic regulatory mechanisms such as *cdc*2-like protein kinases (Rodriguez et al. 1994; Van Dolah et al. 1995). The typical eucaryotic cell cycle initiates with the mitotic division of the cells (M phase) followed by interphase, consisting of three segments, G_1, S, and G_2. During the first segment, G_1, the cells are metabolically very active. The S phase, when DNA synthesis occurs, follows G_1 and extends until chromosome replication occurs and the DNA content of the cell has doubled. The cell then enters G_2, which lasts until mitosis occurs again. When conditions are unfavorable, some cells can withdraw from the regular cell division cycle and enter a reversible cell cycle arrest phase (G_0) during G_1 (Prescott 1976). The time taken to proceed through one complete cell division is the generation time of the cell.

Our objective was to determine the onset of a metabolic process within the cell cycle; thus, all the cells in a culture must proceed through the different stages and divide at the same time. Dinoflagellate division can be phased by photoperiod and occur during a clearly defined interval such as the dark-to-light transition (Chisholm 1981). However, because dinoflagellate growth rates in culture are typically <1 division per day, only a portion of the population will divide over one photoperiod. Cells that are not ready to divide must proceed from their respective positions in the cell cycle through DNA synthesis and, eventually, mitosis during the next or subsequent

[1] Corresponding author.

Acknowledgments

We thank Zheng Lei for technical support during the experiment.

This work was supported by grants from the National Science Foundation (OCE 89-11226 and OCE 94-15536) and a graduate research fellowship from "La Caixa," Spain (GTO).

Contribution 9223 from the Woods Hole Oceanographic Institution.

light period. Measurements on phased cultures thus represent an average of the physiological status of cells in several different metabolic states at the time of sampling (Chisholm 1981). Synchronized cultures are therefore required, yet this is difficult to accomplish with dinoflagellates. Several methods have been used in the past to synchronize dinoflagellates. *Gonyaulax polyedra* was synchronized with a sieving technique that separated cell cycle stages on the basis of cell size (Homma and Hastings 1988). This approach, however, requires excessively large volumes of culture in order to obtain sufficient biomass for the measurements of interest to our study. *Amphidinium carterae* was synchronized by manipulating the length of the light–dark cycle (Galleron and Durrand 1976), a method that did not work with *Alexandrium fundyense* cultures in our hands (unpubl. data).

Alternatively, a block-release approach can be used to synchronize cells. This method is based on the hypothesis that cells arrested by an external factor at a specific point during their cell cycle will proceed through the rest of the cell cycle stages as a homogeneous population after being released from the constraint (Pardee et al. 1978). Such block or transition points have been identified during late G_1 in mammalian cells (Pardee et al. 1978) and yeast (Johnston et al. 1980). Our efforts to locate such points in dinoflagellate cultures using metabolic inhibitors have not been successful, possibly because the cell wall of dinoflagellates is impermeable to many organic molecules or because the autotrophic nature of the organisms does not facilitate uptake of the inhibitors (unpubl. data).

One factor that can arrest cells at a particular point of their cell cycle is light. Light is of primary importance for activating physiological processes as well as determining the timing of cell cycle events in phytoplankton (Chisholm 1981; Vaulot 1985). In phytoplankton, light-dependent block points can be passed by a cell only after it has been exposed to sufficient light. Such transition points have been documented in *Chlamydomonas* (Spudich and Sager 1980), *A. carterae* (Olson and Chisholm 1986), and *Hymenomonas carterii* and *Thalassiosira weisflogii* (Vaulot et al. 1986). If the cells are deprived of the minimal light requirement and there is only one light-dependent transition point, and if the length of dark arrest is equal to or greater than the entire cell cycle (i.e. one generation time), all cells should be blocked at the same point. Once the normal light–dark cycle is restored, a synchronized population is obtained.

In this study, we employed a block-release approach, using prolonged darkness to arrest *A. fundyense* in a light-dependent section of the cell cycle. Cells were released to a normal 14 : 10 L/D cycle, and closely spaced measurements were made to determine the small-scale dynamics of toxin production. The parameters measured included toxin concentration, toxin composition, DNA content, cell size, and total protein.

Materials and methods

The organism—The dinoflagellate *A. fundyense* Balech (strain GtCA29) was used throughout our study. This clonal culture was established in January 1985 from a cyst isolated from Gulf of Maine sediments, 32 km east of Portsmouth, New Hampshire. Before the experiments, cultures were maintained at 15°C in f/2 medium (Guillard and Ryther 1962) modified by addition of H_2SeO_3 (10^{-8} M) and by reducing the concentration of $CuSO_4$ to 10^{-8} M. Vineyard Sound seawater (0.2-μm filtered, 31‰ salinity) was used as the medium base. Throughout the experiment, irradiance of $\sim 150 \times 10^{18}$ quanta s^{-1} m^{-2} was provided by "cool-white" fluorescent bulbs on a 14 : 10 L/D cycle.

Synchronization experiment—Three 20-liter borosilicate glass carboys containing 17 liters of sterile-filtered f/2 medium were inoculated with acclimated exponential phase cells to an initial cell density of ~200 cells ml^{-1}. The cultures were incubated at 20°C and aerated by gentle bubbling with activated-charcoal-filtered air. After completion of the light cycle on the third day after inoculation (~400 cells ml^{-1}), the incubator lights were turned off for a period of 82 h. One hour before the normal 14 : 10 L/D cycle was restored (t_0 of the experiment), samples for toxin, DNA, cell concentration, and protein were taken from each of the carboys. Samples were collected from all three carboys at hours 2, 4, 12, and 18, and every 2 h from hour 22 through 94. The samples were taken from each carboy by blocking the aeration exhaust port of the carboy, thereby pressurizing the vessels and forcing a sample of the culture through a sample tube into the sampling containers. The cells were not mixed manually or disturbed by any other physical means. During the dark period and to ensure that the cultures were not exposed to light, sampling was performed under a 6-W incandescent red light; special precautions were taken to minimize exposure to stray light.

Toxin analysis—Between 2.5 and 5×10^5 cells were collected from the subsamples by centrifugation (3,000×*g*, 23°C). The resulting pellet was rinsed into a centrifuge tube and resuspended in 0.5 M acetic acid for extraction by sonification. The extracts were stored at −20°C before analysis. The extracts were analyzed by HPLC (Oshima et al. 1989) incorporating the modifications previously described by Anderson et al. (1994).

Soluble protein—At least 50,000 cells were collected by centrifugation (3,000×*g*, 23°C) for protein quantification. After aspiration of the supernatant, the pellet was stored frozen at −20°C. For analysis, 1 ml of 0.1 N NaOH was added to the pellet and the suspension sonified for 15 s to disrupt the cells. Samples were then digested for 20 min at 80°C, centrifuged, and the supernatant removed and neutralized with 0.1 volumes of 1.0 N HCl (Binder and Anderson 1990). A 50-μl fraction of the neutralized solution was mixed with 1 ml of bicinchoninic acid (BCA) working solution (Pierce), and the absorbance of duplicate samples determined at 562 nm.

Flow cytometric analysis—A 15-ml aliquot of culture was preserved with 5% Formalin (vol/vol) and stored at 4°C. The cells were centrifuged (1,700×*g*, 23°C, 3 min) and the pellet resuspended in 10 ml of ice-cold methanol and stored at 4°C to extract chlorophyll. The samples were then further concentrated by centrifugation. A subsample of the methanol-pre-

served material was transferred into a 1.5-ml microcentrifuge tube and pelleted at 2,000 rpm. The supernatant was removed and the cells washed with 1 ml of PBS (40 mM Na_2HPO_4, 22 mM KH_2PO_4, 85 mM NaCl). After centrifugation, the pellet was resuspended in 0.5 ml of propidium iodide (PI) staining solution (4 μg ml^{-1} PI, 1,250 units RNaseA ml^{-1}) and allowed to react in the dark for at least 2 h before analysis on an Epics V flow cytometer (Coulter Electronics) (Olson et al. 1986). The results were reduced by running an inside-out and an outside-in model with trapezoidal S phase fitting on ModFit 5.11 (VERITY Software House, Inc).

Cell size—Cell diameter was determined by analyzing unfixed cells (3 ml of the culture) on a Multisizer apparatus (aperture 100 μm) (Coulter Counter Ltd.) within 30 min after sampling. Mean sizes were calculated from the Gaussian distributions obtained.

Cell concentrations—Cell concentrations were determined by counting Utermöhl-preserved samples (Utermöhl 1958). At least 400 cells per sample were counted in a Sedgwick-Rafter counting chamber. Cell densities represent the mean of the averaged triplicate counts for each carboy.

Data fitting—Simple, segmented and smoothed linear models were fitted to the cell growth and toxin concentration data. The fitting program uses the Marquardt-Levenberg algorithm to minimize the sum of the squares of the differences between the equation values and the data (SigmaPlot, Jandel Corp.). This is an iterative process that lasts until the model and the data converge. Convergence is achieved when the absolute value of the difference between the square root of the sum-of-squares of the residuals is <0.0001.

The fitting was done with the equation

$$f_n(t) = kt + N_n. \quad (1)$$

$f(t)$ is a linear function of time, k is the growth rate (or toxin production rate; units: div. h^{-1} and pmol ml^{-1} h^{-1} respectively), and N_n is the cell concentration (or toxin concentration; units: cells ml^{-1} and pmol ml^{-1} respectively) at the end of compartment $n - 1$. If X is a parameter for cell concentration (or toxin concentration), n is the number of the curve segment, and T is a parameter for time at the end points of the different segments, the rate k between T_n and T_{n-1} will be given by

$$k = \frac{X_n - X_{n-1}}{T_n - T_{n-1}}. \quad (2)$$

Because $f(T_n) = X_n$, N_n can be defined as

$$N_n = \frac{X_{n-1}T_n - X_nT_{n-1}}{T_n - T_{n-1}}. \quad (3)$$

Incorporating Eq. 2 and 3 into 1 yields a function $f_n(t)$:

$$f_n(t) = \frac{X_n(T_n - t) + X_{n+1}(t - T_{n-1})}{T_n - T_{n-1}} \quad (4)$$

where $f(t)$ is the linear function of time that describes the changes in cell number (or toxin concentration) in each of the segments on Fig. 1A and B. Initially, the different values for T were arbitrarily specified at the light–dark and dark–light transitions. After several iterations of the model, the time points T defining the beginning and ending of each segment were determined from the best least-square fit to the entire data set. The results were then plotted as a segmented curve together with the actual data.

Abbreviations used throughout are: STX—saxitoxin; NEO—neosaxitoxin; GTX1,2,3,4,5—gonyautoxins 1, 2, 3, 4, and 5; C2—toxin C2; G_0, G_1, and G_2—gap 0, gap 1, and gap 2 phases of the cell cycle; S—synthesis phase; M—mitosis.

Results

All results represent the mean values obtained by averaging data from three independent cultures grown in parallel and started with the same acclimated inoculum.

Synchrony and cell growth—When the dark-arrested cultures were returned to a 10 : 14 L/D cycle, cell numbers remained constant for 18 h, with an average concentration (± SD) of 723(±61) cells ml^{-1} (Fig. 1A). By hour 26 a new stable population size of 1,012(±51) cells ml^{-1} was observed—a 40% increase from initial levels. This was followed 16 h later by a major surge in division, with concentrations doubling to 1,999(±135) cells ml^{-1} in an 8-h interval. This cell density was sustained until hour 66 when a new synchronized division event began that brought the population to 3,465(±142) cells ml^{-1}—a 1.8-fold increase. Cell proliferation always started 3–6 h into the dark phase and lasted for ~9 h.

Linear regressions were calculated for each of the intervals described above. Only the sections delimited by hours 18–26, 42–50, and 66–74 had slopes that were significantly different from zero ($P < 0.001$). The horizontal, nongrowth segments had slopes which were not statistically different from zero ($P > 0.93$, C.I. 97%). These stepwise linear increases in cell concentrations were modeled by fitting a simple, segmented and smoothed linear model to the data (*see materials and methods*). The fitted curve matched the data extremely well, as shown in Fig. 1A.

Cell size distributions—Cell diameter was determined for hours 0 through 56, and three distinct size classes could be distinguished (Fig. 2). At the end of the dark-arrest period, hour 0, the cells had an equivalent spherical diameter (± SD) of 23 μm (±1.2). This peak corresponds to the size of cells in G_0. During the first 24 h these cells increased in size to 29 μm (±1.4), coinciding with a peak in G_1. For the next 8 h their diameter remained constant; it started to increase again at hour 34 and reached a maximum of 33 μm (±1.6) at hour 44, corresponding to the peak of the G_2 + M cell cycle stage. Subsequently, the cells rapidly decreased in size to 29 μm (±1.3).

Protein content—Protein content per cell was 400 pg (±65) in the dark-arrested cells, but increased once the light was restored, exhibiting a typical bimodal pattern through time that peaked at the end of the light periods (hours 15, 39, 63, and 87), and reached minima at the end of the dark periods (hours 25, 49, and 73) (Fig. 3). The minimum was

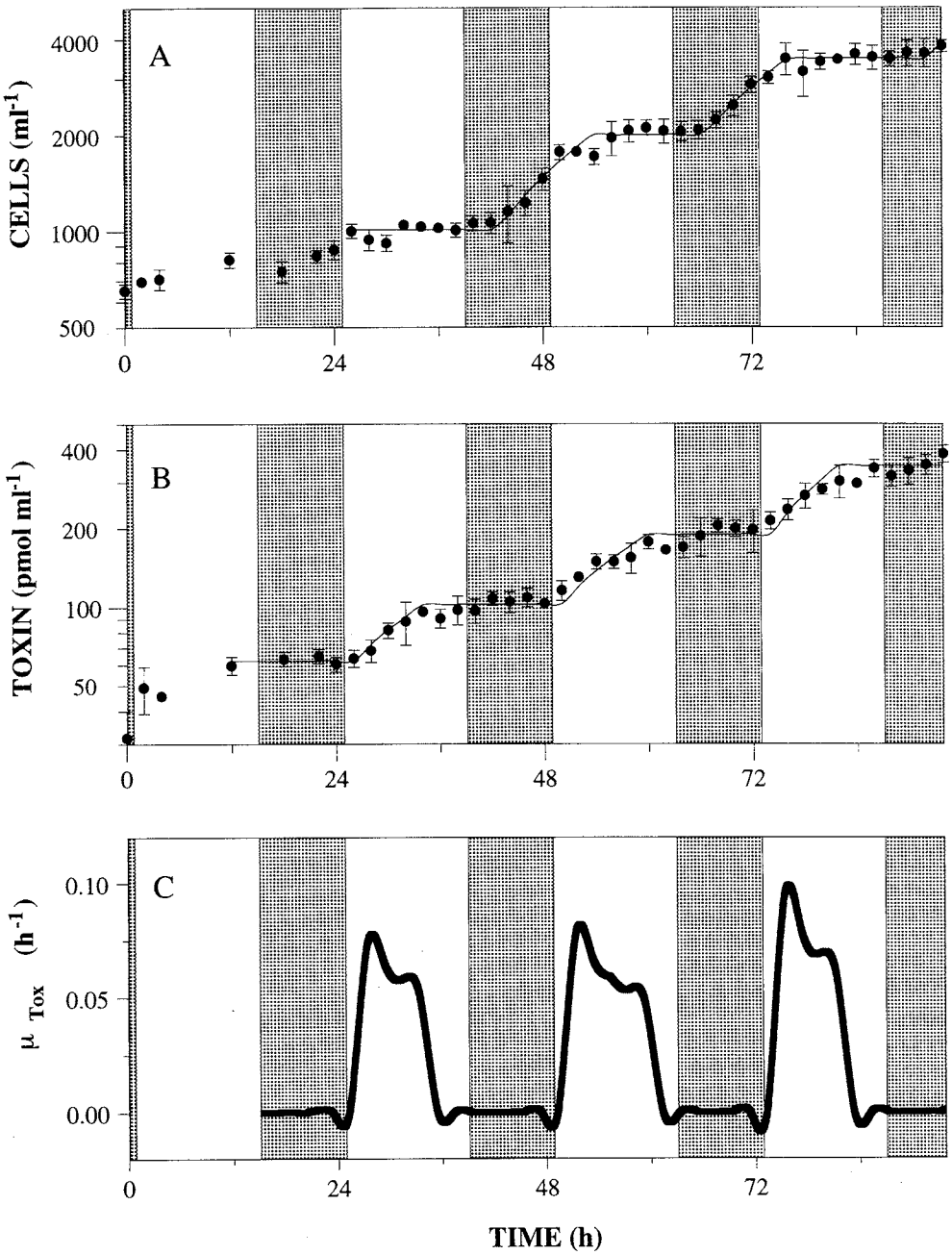

Fig. 1. Cell division pattern, changes in toxin concentration of the population and specific toxin production rates, μ_{Tox}, in *Alexandrium fundyense* as a function of time and during synchronous growth on a 14 : 10 L/D cycle (dark periods indicated by shaded areas). Cell densities (A) and total toxin concentration (B) in the culture measured at 2-h intervals (Error bars denote ± SD). Data were fitted to simple segmented linear models (continuous line; *see text*). Specific toxin production rates (C), μ_{Tox}, were obtained from the fitted curve in panel B (*see text*).

constant at 523 pg (±58). The first maximum, at hour 15, was at only 608 pg (±79). All other maxima were at 1,106 pg (±126).

Cell cycle stages—Two cohorts of cells were apparent in the early stages of the experiment (Fig. 4). The first, comprising ~30% of the total population, appeared 11 h into the first light period, evidenced as an increase in the percentage of cells in S and a concurrent decrease in G_1 cells. Shortly thereafter, a small peak in G_2 + M occurred, after which 96% of the population was in G_1 phase at hour 22. This corresponded to a 30% increase in total cell concentration at that time. The second cohort of cells (the remainder of the cells) did not divide during the first 36 h of the experiment. This larger cohort was arrested in what we can define as G_0 based on DNA content, protein content, toxin content, and cell size (*see discussion*). From the

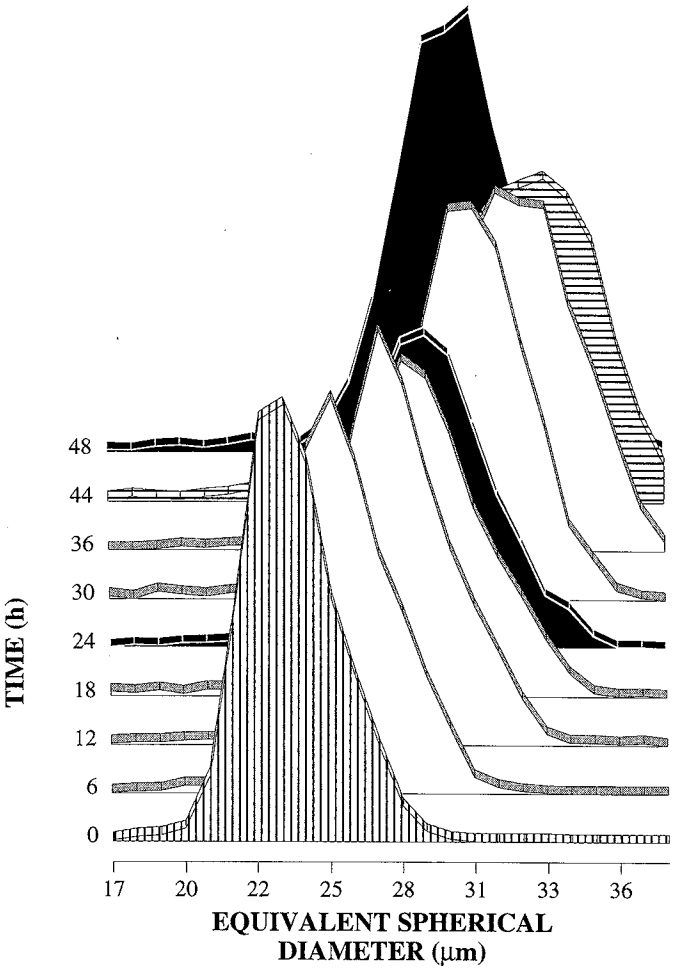

Fig. 2. Variation in the cell size distribution of *Alexandrium fundyense* during the first 48 h of the synchronization experiment (height of areas is equivalent to number of cells). Area with vertical stripes corresponds to cells in G_0 (23±1.2 μm), black areas to G_1 (29±1.4 μm), and the horizontally striped area to G_2 (33±1.6 μm).

beginning of the second L/D cycle on (hour 26), the two populations progressed together through the rest of the cell cycles, as corroborated by the cell cycle patterns (Fig. 4), the cell size distributions (Fig. 2), and the regular increases in cell density (Fig. 1A).

The duration of the cell cycle phases was determined from the variations in DNA content for the duration of the experiment. Assuming that the cells that go first through one cell cycle stage are the ones also going first through the subsequent stages, and after determining the transition times between the peaks corresponding to the different phases (Beck 1978; Yamaguchi and Imai 1994), we calculated G_1 to be ~16 h, the S phase 2 h, and G_2 + M, 6 h. Cells in G_2 and cells undergoing mitosis (M) are regarded as one group because their cytological differences cannot be resolved with flow cytometry.

Toxin content—When the culture was removed from the dark and the normal light–dark cycle re-established, the total toxin in the culture [toxin ml^{-1} (± SD)] increased from 32(±8) pmol ml^{-1} to 62.4(±2.2) in a period of 8 h and then remained stable for 16 h. Following this, we observed a new surge in toxin production at the beginning of the light period at hour 25. This increase continued for 8 h, reaching a new constant level of 102.6(±7.7) pmol ml^{-1}. We observed the same pattern of toxin increase and plateau during the subsequent L/D cycles, with stable concentrations of 189(±17.5) and 347.4(±40.8) pmol ml^{-1} respectively. The mean increase in concentration during each interval toxin production was 90%. This pattern of toxin production coincides with the dynamics of toxin accumulation per cell as exemplified in Fig. 5 for hours 20 through 54. Toxin content per cell, as calculated from toxin concentrations in the culture and the corresponding cell densities, followed a regular pattern of increase, stabilization, and decrease throughout each generation time.

Linear regressions were calculated for each of the segments described in the toxin per milliliter data. Only the sections delimited by hours 1–12, 26–34, 48–60, and 72–82 had slopes that were significantly different from zero ($P < 0.001$). The

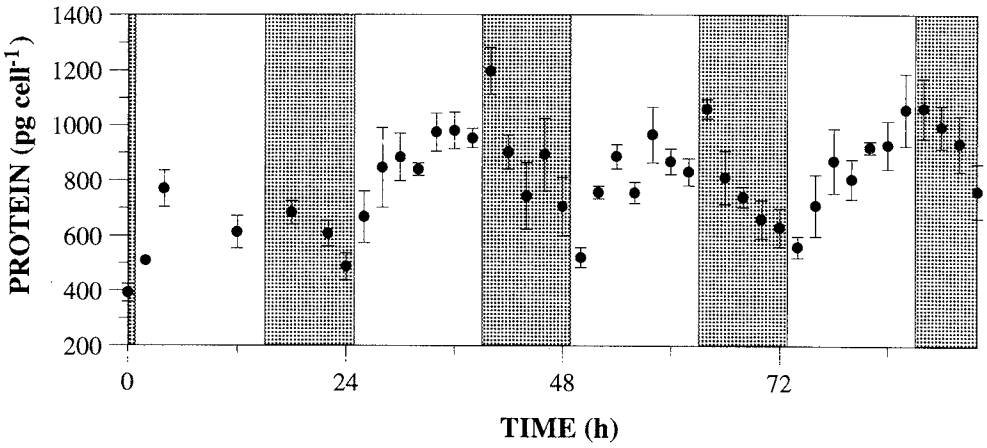

Fig. 3. Protein production in *Alexandrium fundyense* as a function of time and during synchronous growth on a 14:10 L/D cycles (dark periods shown shaded). Protein content was measured at 2-h intervals (error bars denote ± SD).

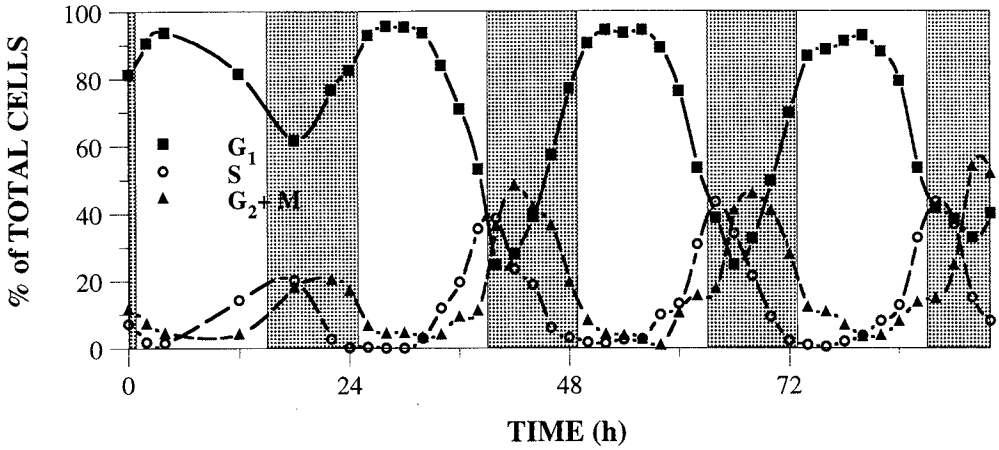

Fig. 4. Relative distribution of *Alexandrium fundyense* cells in the different cell cycle stages as a function of time and during synchronous growth on a 14:10 L/D cycle (dark periods shown shaded). The different cell cycle stage fractions represent the percentage of total cells in each phase and were determined by analysing the varying amounts of DNA per cell (C.V. ≤ 5%). Error bars not shown for clarity.

horizontal, nonproduction segments had slopes that were not statistically different from zero ($0.9 > P > 0.57$, C.I. 89%). These stepwise linear increases in toxin concentrations were modeled by fitting a simple, segmented and smoothed linear model to the data (*see materials and methods*). In this case, X was the parameter for toxin concentration (Fig. 1B). The fitted curve is plotted with the data in Fig. 1B.

Specific toxin production rates—The specific toxin production rate, μ_{Tox}, was defined as the change in toxin concentration relative to the existing concentration in the synchronized cultures. This definition is based on the previously described specific toxin production rate in asynchronous cultures, μ_{Tox} (d^{-1}) (Anderson et al. 1990*b*). The rates were obtained with the equation

$$\mu_{Tox} = \frac{\ln\left(\frac{T_1}{T_0}\right)}{t_1 - t_0}. \quad (5)$$

μ_{Tox} is the specific toxin production rate (h^{-1}) and T_1 and T_0 are the toxin concentrations at times t_1 and t_0 as obtained from the fitted curve in Fig. 1B. A regular pattern of toxin production is revealed (Fig. 1C), in which toxin production rates are positive for a period of ~8 h and then drop to zero for the remaining 16 h of the cell cycle.

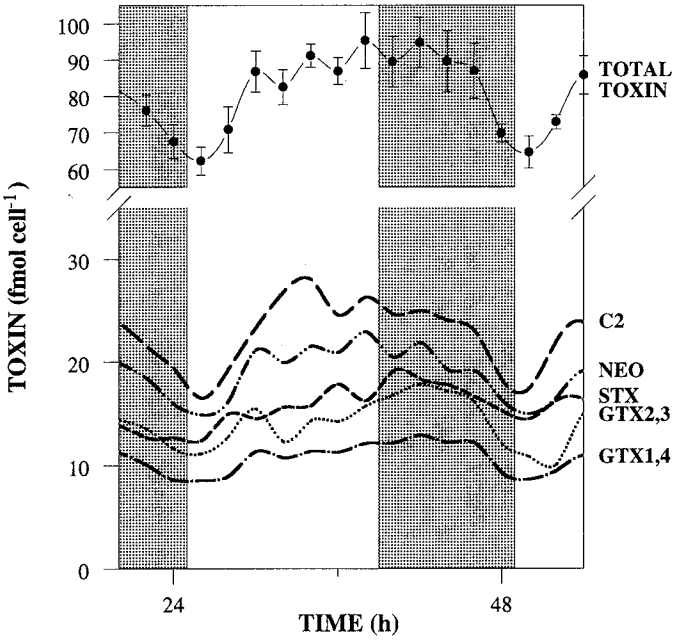

Fig. 5. Changes in total toxin composition per cell of *Alexandrium fundyense* as a function of time and during synchronous growth on a 14:10 L/D cycle (dark periods shown shaded). The Y-axis is discontinuous between 35 and 55 fmol cell^{-1}. Error bars are not plotted for the single toxin derivatives for sake of clarity.

Toxin composition—The relative proportions (mole percent of total toxin) of the five main saxitoxins remained essentially unchanged throughout the experiment (data not shown). The accumulation patterns of the seven main derivatives of saxitoxin (C2, NEO, STX, GTX2,3 isomers, and GTX1,4 isomers) were very similar (Fig. 5). Analysis of the exact onset of accumulation for each of the toxins suggests that C2 increases first, followed by STX and the isomeric pair GTX2,3. The concentrations of NEO and the pair GTX1,4 begin to increase ~1–2 h later.

Discussion

This study documents for the first time the extent to which the toxicity of the dinoflagellate *A. fundyense* varies on short (hourly) time scales. The fluctuations in toxin production were evaluated in the context of the cell cycle, a framework that allowed us to divide one cell generation into a series of shorter stages that could easily be delineated using DNA measurements. Synchronization of the cells ensured that virtually the entire population was in the same physiological

state at each sampling point and therefore that the results of the analysis of the population as a whole could be extrapolated to the individual cell.

Synchrony and growth patterns—Immediately after release from the dark, *Alexandrium* shows a lag-phase equivalent to one generation time. Such nonproliferation periods, previously described for induced synchrony in yeast and other eucaryotes (Mitchison 1969; Pardee et al. 1978), are the result of a G_0-like segment in the cell cycle that prevents the cells from progressing through G_1 and dividing. The cells in this stage are of smaller size (Fig. 2). After a period of 24 h the cells regain the normal size of ~30-μm diameter for this species (Fig. 2) with 96% of the cells being in G_1 (Fig. 4). During the next 24 h cell size increases to reach a maximum during the peak of G_2 (Figs. 2 and 4). Thereafter the cells decrease rapidly in size to values equivalent to G_1 cells. The smaller size correlated to cells in G_0 is never seen again during the experiment. These data suggest the presence of a size-dependent transition point at the end of G_1, similar to other eucaryotes (Mitchison et al. 1991). The degree of synchrony achieved in the two subsequent divisions, as determined from the relative proportions of cells in the different cell cycle stages and the increase in cell numbers (Figs. 3 and 1A), was 100 and 90% respectively. Two further divisions (data not shown) show increments of 89 and 80%. These numbers imply that even though synchrony was achieved during the first proliferation step, it was progressively lost. Similar patterns have been previously described for other eucaryotes such as yeast (Mitchison et al. 1991). The most widely accepted explanation for this loss of synchrony is that the cells are growing at their maximum possible growth rate—a situation that is not sustainable as the cells are not in balanced growth, when uptake equals metabolic needs (Mitchison 1969). A similar situation is true for *A. fundyense*. This species usually grows at a rate of 0.3–0.5 divisions per day in culture, yet under the specific conditions of our experiment, the cells were forced into dividing once per day—a pace that is not sustainable over long periods of time. Such explosive growth events, during which populations of organisms can grow very fast, may be a mechanism for bloom formation (T. Smayda pers. comm.).

Temporal pattern in toxin production—In analyzing the variability in toxin production during this study, we chose to focus on two parameters. First, the variations of toxin per unit volume of culture (toxin ml^{-1}) were determined, for this parameter is an indicator of net toxin production and should never decrease unless toxin is catabolized or leaked from the cell. Secondly, toxin per cell was derived from the previous data to follow the dynamics of toxin accumulation on a per cell basis (note that we use the term "toxin production" to mean toxin accumulated in the cell, ignoring losses due to leakage or catabolism). The most important conclusion from the data presented here is that toxin production is induced by light and occurs in a defined interval within the G_1 phase of the cell cycle. Specific toxin production rates were positive for a period of 8–10 h in early G_1 and remained zero for the remainder of the interphase and mitosis (Fig. 1C), 6 h of which were still in light. This behavior was not only observed once the population was synchronized but also during the first 24 h when the cells were not yet progressing through the regular cell cycle.

If toxin were produced continuously and at a constant rate, toxin per milliliter should increase exponentially through time. In Fig. 1B, this would plot as a straight line with constant slope. Instead, the data reveal a steplike pattern similar in form to the steps seen in cell number when counted at closely spaced intervals through time (Fig. 1A). This is further confirmed when toxin accumulation per cell is analyzed, as exemplified in Fig. 5. Toxin accumulates (is produced) over a period of 8–10 h before its concentration reaches a constant value. This level is maintained until the cells start dividing (Fig. 1A) and the toxin is most probably partitioned between the two daughter cells (Fig. 5) because toxin concentration in the culture does not change during mitosis (Fig. 1B). The average increase in toxin concentration during the experiment is exponential but is determined by an hourly scale, steplike pattern of toxin production. Such discontinuous production or activity patterns in synchronized cultures have been previously described in other organisms and are universal for cellular processes that are activated by external or internal factors rather than being continuous throughout the cell cycle (Mitchison 1969).

Given this discontinuous pattern of toxin production and increase in cell concentration, we decided to fit a segmented linear model to each of the data sets. The underlying assumption was that the production rate, similarly to the growth rate, follows a Gaussian distribution during the accumulation or doubling periods, resulting in a sigmoidal curve for the increase in toxin concentration or cell number (Mitchison 1969; Vaulot 1985). For simplicity purposes, such sigmoidal curves can be approximated by a straight line. The slope of this straight line would represent the mean production rate or growth rate during that period. Initially, the time points (parameter *T, see materials and methods*) delimiting each segment of the cell or the toxin concentration curve on Fig. 1A and B were arbitrarily defined at the times when the lights went on or off. After several iterations, the time intervals defining the segments were adjusted through a least-square, best-fit to the data. The duration and timing of each segment thus determined closely matched the segments we had originally determined for calculating the slopes (Fig. 1A, B) and, in the case of toxin production, the model also coincided with the patterns observed in toxin accumulation per cell (Fig. 5). These results confirmed that toxin production occurred during an 8–12-h interval in early G_1.

Specific toxin production rates were obtained using the values from the fitted curve in Fig. 1B. A regular pattern of toxin production is revealed in which toxin production rates are positive for a period of ~8–10 h and then drop to zero for the remaining 16 h of the cell cycle (Fig. 1C). In the three consecutive cycles we analyzed, toxin production was induced by light at the beginning of the light period and stopped ~8–10 h into G_1.

Protein production did not mimic toxin production throughout time (Fig. 3). Accumulation of soluble protein was also induced by light, but it continued during the light period and was reversed with the beginning of the dark pe-

riod. Identical protein accumulation dynamics have been reported in other phytoplankton (Howell et al. 1977; Hastings et al. 1981; Puiseux-Dao 1981).

We conclude from these data that—unlike protein production—which extends for the entire interphase comprising G_1, S, and G_2 and is solely dependent on light, toxin production is induced by light, is confined to an early portion of the G_1 phase only, and ceases before the light phase ends.

Light induction—It has been postulated earlier that toxin production can be influenced by light. *Alexandrium* (=*Protogonyaulax*) *tamarense* was shown to increase its toxicity when the growth rate was reduced by decreasing light intensity (Ogata et al. 1987). This result is analogous to those obtained when growth rates are reduced as a result of nutrient limitation (Proctor et al. 1975; Hall 1982; Boyer et al. 1985; Anderson et al. 1990*b*) or temperature (Hall 1982; Ogata et al. 1987; Anderson et al. 1990*b*). Furthermore, a direct correlation between specific growth rates and specific toxin production rates during the exponential phase in semicontinuous cultures has been observed, suggesting a possible relationship between toxin production and the cell cycle (Anderson et al. 1990*b*). These observations can be explained taking into consideration our results that show that toxin production is clearly induced by light, lasts only for 8–10 h and is confined to the early G_1 phase (Figs. 1C and 4). Cells of the dinoflagellate *A. carterae* growing at a slow rate do so by increasing the duration of the G_1 phase while keeping the length of the other phases relatively constant (Olson and Chisholm 1986). If a cell is arrested in G_1 for several L/D cycles it could undergo several rounds of toxin synthesis before dividing, thereby increasing its toxin content and becoming more toxic.

Toxin composition—Another aspect of toxin production in *A. fundyense* is the relative composition of its toxin pool. It has been reported in the literature that the toxin composition of an individual isolate of *Alexandrium* remains constant under a variety of environmental conditions as well as through the different culture growth stages (Hall 1982; Boyer et al. 1987; Cembella et al. 1987; Ogata et al. 1987). Recently, however, significant changes in toxin composition have been reported in cells exposed to different stresses. The relative abundance of STX in *A. tamarense* and *Alexandrium catenella* has been shown to decrease as the cells enter plateau phase and stop growing (Boczar et al. 1988). *A. fundyense* shows an increase in STX content at higher specific growth rates (Anderson et al. 1990*a*), which is consistent with the results of Boczar et al. (1988) for *A. tamarense* and *A. catenella.*

Our study also documents changes in toxin composition in *A. fundyense,* but these variations occurred at different time scales from those in previous studies. Although the relative proportions (mole percent of total toxin) of the five main saxitoxins remained essentially unchanged throughout the experiment (data not shown), the accumulation patterns (pmol $cell^{-1}$) of the seven main derivatives of saxitoxin, showed slight variations with respect to the timing of formation (Fig. 5). Analysis of the exact onset of accumulation for each of the toxins suggests that C2 starts to build first, followed by STX and the isomeric pair GTX2,3. With a delay of ~1–2 h, the concentrations of NEO and the pair GTX1,4 begin to increase. A plausible interpretation of these results would involve a biosynthetic pathway consisting of one precursor centered around C2 and several subsequent transformation steps (Fig. 6). First, C2 would be transformed into GTX2,3 by means of an *N*-sulfatase. In a second step, GTX2,3 could be further transformed into STX by another sulfatase. Finally, a hydroxylase adds an *N*-hydroxy group to GTX2,3 and STX, turning them respectively into GTX1,4 and NEO. The rough kinetics of the transformations, as derived from Fig. 5, would fit in such a putative scheme. These pathways are largely speculative at this stage. The synchronization of cultures and closely spaced toxin analysis shows promise for elucidating the kinetic profiles of the individual toxin productions.

A similar scheme of the STX biosynthetic pathway has been outlined before (Shimizu 1993), but no experimental evidence had been gathered before our study. This interpretation has to be carefully contrasted with observations of changes and variations in toxin composition in other dinoflagellate species such as *Pyrodinium bahamense* and *Gymnodinium catenatum* (Oshima et al. 1993; Usup et al. 1994). In these organisms, STX has been postulated to be a precursor or parent compound that is rapidly converted into NEO or GTX5, as these last two compounds are predominant and only negligible amounts of STX are detected (Oshima et al. 1993; Usup et al. 1994). In an integrated sheme of the STX biosynthetic pathway, interconversions among the toxins would be determined in part by the presence or absence of the appropriate enzymes, but actual toxin production would be the result of the accumulation of only one precursor or parent compound. This precursor could be one of the toxins or another unknown compound. Studies similar to this one using dinoflagellates that differ in their overall toxin composition are necessary to more conclusively elucidate the STX biosynthetic pathway.

Cell cycle—Our original purpose was to investigate short-term variability in toxicity in *A. fundyense,* but it also revealed some interesting aspects of the cell cycle of this species and the manner in which the cells respond to prolonged darkness. DNA synthesis in dinoflagellates has been reported to be continuous throughout the cell cycle in several species (Karentz 1983; Rizzo 1987) or confined to a discrete S phase in others (Chang and Carpenter 1988; Yamaguchi 1992). *A. fundyense* clearly synthesizes DNA during a discrete time period, phased to a specific portion of the cell cycle (Fig. 4). This S phase takes place during the latter portion of the light period and extends into the early dark period (Fig. 7).

An interesting observation relates to the presence of two cohorts of cells at the onset of the experiment and the subsequent homogeneity of the population several L/D cycles later. This can be explained by the presence of two transition points in G_1. Cells arrested at the first, light-dependent transition point (in early G_1, immediately after mitosis) proceed through a G_0-like period associated with lower metabolic activity and smaller size (Figs. 2 and 5). In addition, a small portion of the population (~20%) was apparently arrested at a transition point located further into G_1 and in this case

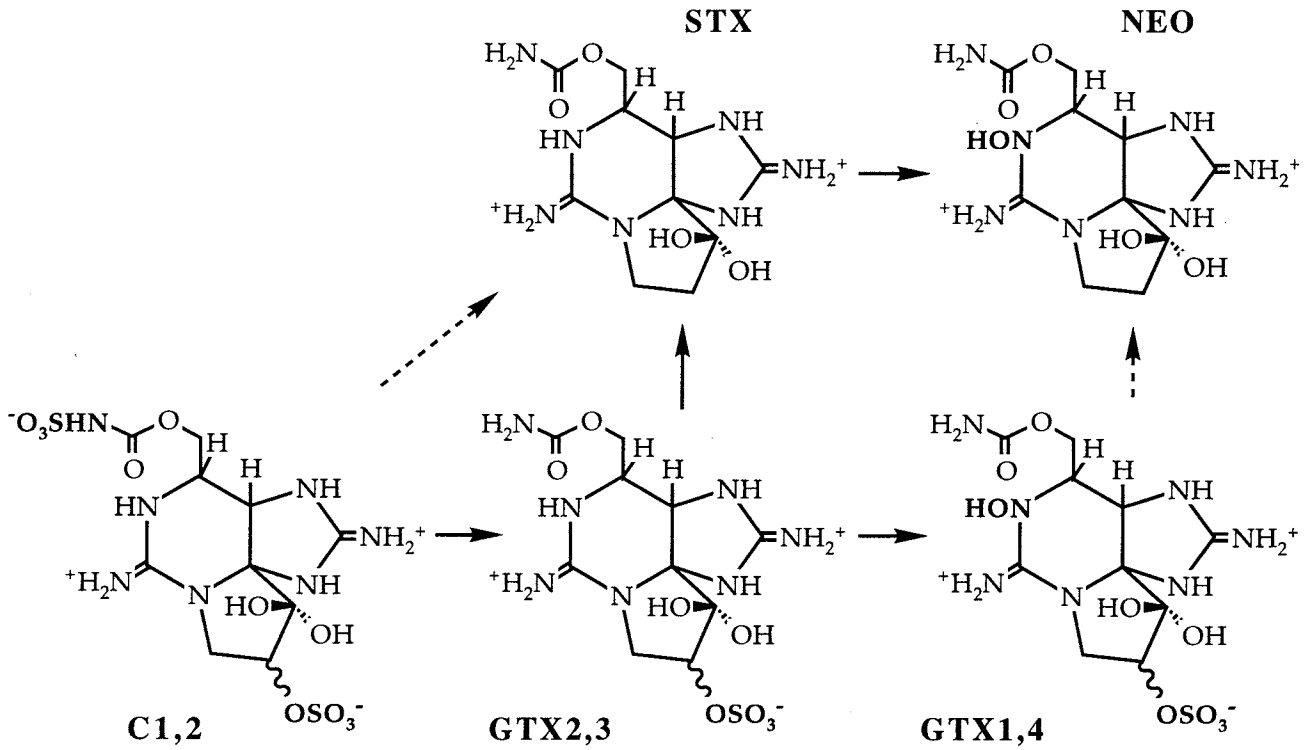

Fig. 6. Putative sequence of events in the biosynthesis of STX and its derivatives. Continuous lines represent most likely interconversions, as deduced from Fig. 5 (*see discussion*). Dashed lines represent other possible paths.

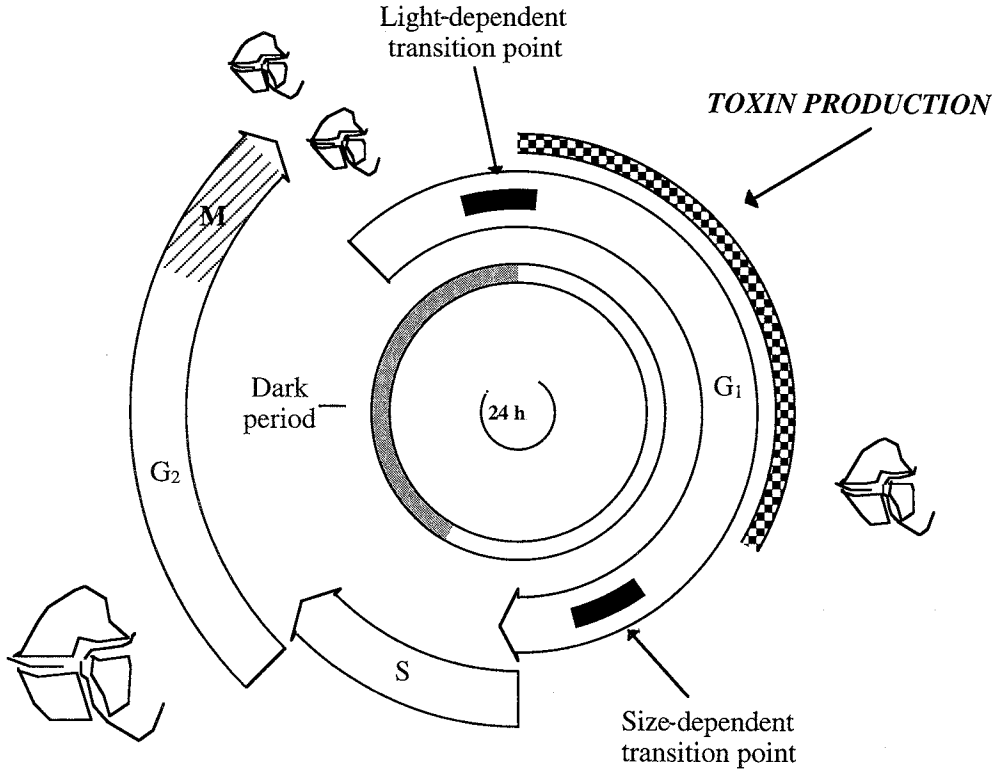

Fig. 7. Diagrammatic representation of cell cycle events in *Alexandrium fundyense* cells during synchronous growth on a 14 : 10 L/D cycle. Open bar—light phase; G_1—gap 1 (postmitotic); S—DNA synthesis phase; G_2—gap 2 (premitotic); M—mitosis.

size-dependent. These cells were slightly larger than the mean of the cells at the beginning of the experiment (Fig. 2) and account for the surge in S phase and G_2 + M cells and the concurrent increase in cell concentration during the dark period of the first L/D cycle (Figs. 1A and 3). Subsequently the entire population doubled over the next L/D cycle. This means that all the cells had become synchronized and were proceeding through the cell cycle as a single unified cohort. In two subsequent L/D cycles cell densities increased by a factor of 1.8 and 1.7 (Fig. 1A). This might indicate a gradual loss of synchronicity in the culture, but the cell cycle information shown in Fig. 3 indicates that the level of synchronicity was still at ~96%. Another explanation for the lack of complete doubling in cell numbers could be the loss of an undetermined number of cells from the sampled population. From the second day on we could observe a cell deposit at the bottom of all three carboys that was difficult to resuspend without damaging the cells.

Single, light-dependent transition points in G_1 have been identified in *Chlamydomonas* (Spudich and Sager 1980) and in *A. carterae* and *H. carterii* (Olson and Chisholm 1986; Vaulot et al. 1986). Two light-dependent transition points have been characterized in *T. weisflogii,* one in G_1 and another in G_2 (Vaulot et al. 1986). A single nutrient-dependent control point located in G_1 has also been identified in *Prorocentrum minimum* (Antia et al. 1990), and the simultaneous presence of nutrient-dependent control points in G_1 and in G_2 has been described in *Oxyrrhis marina* (Whiteley et al. 1993). To our knowledge, the data presented here are the first evidence in phytoplankton suggesting that there may be two different transition points in G_1, one light-dependent and the other size-dependent.

An alternative explanation for the existence of two cohorts of cells at the beginning of the experiment that does not require two transition points in G_1 is suggested by the cell cycle mode of Klevecz (Klevecz 1976), who noted that certain mammalian cell lines had generation times that tended to be integer multiples of 4 h. In the Klevecz model, G_1 is replaced by a loop called G_q which has a duration equal to the quantized intervals between generation times. G_q can thus be viewed as a subcycle from which the cells can re-enter the remainder of the cell cycle, but only after completely traversing G_q one or more times. Because exit from G_q is regulated by environmental factors such as light, the net effect of prolonged darkness would be for a population of cells to be separated into two or more groups depending upon the number of G_q subcycles they had traversed when darkness was imposed. Evidence for quantized generation times in the diatom *Thalassiosira fluvialitis* has been described, but the distribution of generation times for that species was not consistent with the Klevecz model (Chisholm and Costello 1980). In the case of *A. fundyense,* such a model cannot be dismissed, but the data presented here would imply a G_q of 24 h. Therefore, a model of the cell cycle that integrates a light-dependent and a size-dependent transition points seems to be the easiest way to explain our observations (Fig. 7).

Conclusions

Our study documents for the first time the dynamics of toxin production during the cell cycle of *A. fundyense* (Fig. 7). Toxin production was shown to occur over a discrete period during G_1 and to be induced by light. The cell cycle contains two transition points responsible for regulating the passage of the cell through G_1 (light-dependent) and the transition from G_1 to S (size-dependent), respectively. We also suggest that C2 is the first derivative accumulating in the biosynthetic pathway of the toxins in our *A. fundyense* isolate, being subsequently transformed into the other toxins. The restriction of toxin production to a relatively short segment of the cell cycle provides a tool for comparing cells that are and are not synthesizing toxin. This has important implications with respect to the search for genes or enzymes involved in toxin production and their regulation in *Alexandrium.* In this context, work is in progress in our laboratory to identify toxin-specific genes by differential display analysis (Liang and Pardee 1992) of messenger-RNA components of cells harvested at different points during their cell cycle. In general, the work presented here shows that studying dinoflagellates at a high temporal resolution and under synchronized conditions can be useful to gain a broader understanding of their biochemistry and physiology.

References

ANDERSON, D. M. 1989. Toxic algal blooms and red tides: A global perspective, p. 11–16. *In* Red tides: Biology, environmental science, and toxicology. Proc. 1st Int. Symp. on Red tides. Elsevier.

———. 1990. Toxin variability in *Alexandrium* species, p. 41–51. *In* Toxic marine phytoplankton: Proc. 4th Int. Conf. Elsevier.

———, D. M. KULIS, G. J. DOUCETTE, J. C. GALLAGHER, AND E. BALECH. 1994. Biogeography of toxic dinoflagellates in the genus *Alxandrium* from the northeastern United States and Canada. Mar. Biol. **120:** 467–478.

———, ———, J. J. SULLIVAN, AND S. HALL. 1990*a*. Toxin composition variations in one isolate of the dinoflagellate *Alexandrium fundyense.* Toxicon **28:** 885–893.

———, ———, ———, ———, AND C. LEE. 1990*b*. Dynamics and physiology of saxitoxin production by the dinoflagellates *Alexandrium* spp. Mar. Biol. **104:** 511–524.

ANTIA, J. R., E. J. CARPENTER, AND J. CHANG. 1990. Species-specific phytoplankton growth rates via diel DNA synthesis cycles. Accuracy of growth rates measurement in the dinoflagellate *Prorocentrum minimum.* Mar. Ecol. Prog. Ser. **63:** 273–279.

BECK, H. P. 1978. A new analytical method for determining duration of phases, rate of DNA synthesis and degree of synchronization data on synchronized cell populations. Cell Tissue Kinet. **11:** 139–148.

BINDER, B. J., AND D. M. ANDERSON. 1990. Biochemical composition and metabolic activity of *Scrippsiella trochoidea* (dinophyceae) resting cysts. J. Phycol. **26:** 289–298.

BOCZAR, B. A., M. A. BEITLER, J. LISTON, J. J. SULLIVAN, AND R. A. CATTOLICO. 1988. Paralytic shellfish toxins in *Protogonyaulax tamarensis* and *Protogonyaulax catenella* in axenic culture. Plant Physiol. **88:** 1285–1290.

BOYER, G. L., J. J. SULLIVAN, R. J. ANDERSEN, P. J. HARRISON, AND F. J. R. TAYLOR. 1987. Effects of nutrient limitation on toxin production and composition in the marine dinoflagellate *Protogonyaulax tamarensis.* Mar. Biol. **96:** 123–128.

———, ———, P. J. HARRISON, AND F. J. R. TAYLOR. 1985. Toxin production in three isolates of *Protogonyaulax* sp., p. 281–286. *In* Toxic dinoflagellates: Proc. 3rd Int. Conf. Elsevier.

CEMBELLA, A. D., J. J. SULLIVAN, G. L. BOYER, F. J. R. TAYLOR, AND R. J. ANDERSEN. 1987. Variation in paralytic shellfish toxin composition within the *Protogonyaulax tamarensis/catenella* species complex: Red tide dinoflagellates. Biochem. Syst. Ecol. **15:** 171–186.

CHANG, J., AND E. J. CARPENTER. 1988. Species specific phytoplankton growth rates via diel DNA synthesis cycles. 2 DNA quantification and model verification in the dinoflagellate *Heterocapsa triquetra.* Mar. Ecol. Prog. Ser. **44:** 287–296.

CHISHOLM, S. W. 1981. Temporal patterns of cell division in unicellular algae, p. 150–181. *In* Physiological bases of phytoplankton ecology. Can. Bull. Fish. Aquat. Sci. 210.

———, AND J. C. COSTELLO. 1980. Influence of environmental factors and population composition on the timing of cell division in *Thalassiosira fluvialitis.* J. Phycol. **16:** 375–383.

GALLERON, C., AND A. M. DURRAND. 1976. Synchronization of the marine dinoflagellate *Amphidinium carterii* in dense cultures. J. Phycol. **12:** 69–73.

GUILLARD, R. R. L., AND J. H. RYTHER. 1962. Studies of marine phytoplanktonic diatoms. *Cyclotella nana* Hustedt and *Detonula confervacea* (Cleve) Gran. Can. J. Microbiol. **8:** 229–239.

HALL, S. 1982. Toxins and toxicity of *Protogonyaulax* from the northeast Pacific. Ph.D. thesis, Univ. Alaska.

HALLEGRAEFF, G. M. 1993. A review of harmful algal blooms and the apparent global increase. Phycologia **32:** 79–99.

HASTINGS, J. W., J. DUNLAP, AND W. TAYLOR. 1981. Protein synthesis and protein turnover in circadian cycles, p. 519–529. *In* B. Horecker and E. Stadtman [eds.], Current topics in cellular regulation. V. 18. Academic.

HOMMA, K., AND J. W. HASTINGS. 1988. Filtration-selection of cell cycle synchronized *Gonyaulax polyedra*: Quantized generation times. J. Biol. Rhythms **3:** 49–58.

HOWELL, S. H., J. W. POSAKONY, AND K. R. HILL. 1977. The cell cycle program of polypeptide labelling in *Chlamydomonas reinhardtii.* J. Cell Biol. **72:** 223–230.

JOHNSTON, G. C., R. A. SINGER, S. O. SHARROW, AND M. L. SLATER. 1980. Cell division in the yeast *Saccharomyces cerevisiae* growing at different rates. J. Gen. Microbiol. **118:** 479–484.

KARENTZ, D. 1983. Patterns of DNA synthesis and cell division in marine dinoflagellates. J. Protozool. **30:** 581–588.

KLEVECZ, R. R. 1976. Quantized generation time in mammalian cells as an expression of the cellular clock. Proc. Natl. Acad. Sci. **73:** 4012–4016.

LIANG, P., AND A. B. PARDEE. 1992. Differential display of eukaryotic messenger RNA by means of the polymerase chain reaction. Science **257:** 967–971.

MARANDA, L., D. M. ANDERSON, AND Y. SHIMIZU. 1985. Comparison of toxicity between populations of *Gonyaulax tamarensis* of eastern North American waters. Estuarine Coastal Shelf Sci. **21:** 401–410.

MITCHISON, J. M. 1969. Enzyme synthesis in synchronous cultures. Science **165:** 657–663.

———, J. CREANOR, AND B. NOVAK. 1991. Coordination of growth and division during the cell cycle of fission yeast. Cold Spring Harbor Symp. Quant. Biol. **56:** 557–565.

OGATA, T., M. KODAMA, AND T. ISHIMARU. 1987. Toxin production in the dinoflagellate *Protogonyaulax tamarensis.* Toxicon **25:** 923–928.

OLSON, R. J., AND S. W. CHISHOLM. 1986. Effects of light and nitrogen limitation on the cell cycle of the dinoflagellate *Amphidinium carteri.* J. Plankton Res. **8:** 785–793.

———, D. VAULOT, AND S. W. CHISHOLM. 1986. Effects of environmental stresses on the cell cycle of two marine phytoplankton species. Plant Physiol. **80:** 918–925.

OSHIMA, Y., S. I. BLACKBURN, AND G. M. HALLEGRAEFF. 1993. Comparative study on paralytic shellfish toxin profile of the dinoflagellate *Gymnodinium catenatum* from three different countries. Mar. Biol. **116:** 471–476.

———, K. SUGINO, AND T. YASUMOTO. 1989. Latest advances in HPLC analysis of paralytic shellfish toxins, p. 319–326. *In* Mycotoxins and phycotoxins: Proc. 7th Int. IUPAC Symp.

PARDEE, A. B., R. DUBRON, J. L. HAMLIN, AND R. F. KLEVTZIEN. 1978. Animal cell cycle. Annu. Rev. Bochem. **47:** 715–750.

PRESCOTT, D. M. 1976. Reproduction in eukaryotic cells. Academic.

PROCTOR, N. H., S. L. CHAN, AND A. J. TREVOR. 1975. Production of saxitoxin by cultures of *Gonyaulax catenella.* Toxicon **13:** 1–9.

PUISEUX-DAO, S. 1981. Cell-cycle events in unicellular algae, p. 130–149. *In* Physiological bases of phytoplankton ecology. Can. Bull. Fish. Aquat. Sci. 210.

RIZZO, P. J. 1987. Biochemistry of the dinoflagellate nucleus, p. 143–173. *In* F. J. R. Taylor [ed.], The biology of dinoflagellates. Blackwell.

———. 1991. The enigma of the dinoflagellate chromosome. J. Protozool. **38:** 246–252.

RODRIGUEZ, M., J. W. CHO, H. W. SAUER, AND P. J. RIZZO. 1994. Evidence for the presence of *cdc*2-like protein kinase in the dinoflagellate *Cryptecodinium cohnii.* J. Eukaryotic Microbiol. **40:** 91–96.

SHIMIZU, Y. 1993. Microalgal metabolites. Chem. Rev. **93:** 1685–1698.

SPUDICH, J., AND R. SAGER. 1980. Regulation of *Chlamydomonas* cell cycle by light and dark. J. Cell Biol. **85:** 136–145.

USUP, G., D. M. KULIS, AND D. M. ANDERSON. 1994. Growth and toxin production of the toxic dinoflagellate *Pyrodinium bahamense* var. *compressum* in laboratory cultures. Nat. Toxins **2:** 254–262.

UTERMÖHL, H. 1958. Zur Vervoll-commnung der quantitativen Phytoplankton-methodik. Mitt. Int. Ver. Theor. Angew. Limnol. 9. 38 p.

VAN DOLAH, F. M., T. A. LEIGHFIELD, H. D. SANDEL, AND C. K. HSU. 1995. Cell division in the dinoflagellate *Gambierdiscus toxicus* is phased to the diurnal cycle and accompanied by activation of the cell cycle regulatory protein *cdc*2 kinase. J. Phycol. **31:** 395–400.

VAULOT, D. 1985. Cell cycle controls in marine phytoplankton. Ph.D. thesis, Woods Hole Oceanogr. Inst.-Mass. Inst. Technol.

———, R. J. OLSON, AND S. W. CHISHOLM. 1986. Light and dark control of the cell cycle in two marine phytoplankton species. Exp. Cell Res. **167:** 38–52.

WHITE, A. W. 1978. Salinity effects on growth and toxin content of *Gonyaulax excavata,* a marine dinoflagellate causing paralytic shellfish poisoning. J. Phycol. **14:** 475–479.

WHITELEY, A. S., P. H. BURKILL, AND M. A. SLEIGH. 1993. Rapid method for cell cycle analysis in a predatory marine dinoflagellate. Cytometry **14:** 909–915.

YAMAGUCHI, M. 1992. DNA synthesis and the cell cycle in the noxious red-tide dinoflagellate *Gymnodinium catenatum.* Mar. Biol. **112:** 191–198.

———, AND I. IMAI. 1994. A microfluorometric analysis of nuclear DNA at different stages in the life history of *Chattonella antiqua* and *Chattonella marina* (Raphidopyceae). Phycologia **33:** 163–170.